Vacuum space-charge effects in solid-state photoemission

S. Hellmann, K. Rossnagel, M. Marczynski-Bühlow, and L. Kipp
Institute for Experimental and Applied Physics, University of Kiel, D-24098 Kiel, Germany
(Received 24 September 2008; revised manuscript received 4 December 2008; published 5 January 2009; publisher error corrected 28 January 2009)

Solid-state photoemission spectroscopy relies to a large part on pulsed photon sources: third-generation synchrotron-radiation sources and ultrafast laser systems in particular. Especially when the photon pulses are intense, Coulombic repulsion between the emitted electrons will be a limiting factor for photoemission experiments aiming at highest energy and angle resolutions. In the present work, the propagation of the photoelectron cloud to the detector is studied with a full *N*-body numerical simulation. The influence of various parameters, in particular number of electrons per pulse, source size, pulse duration, kinetic-energy and emission-angle distributions as well as presence of mirror charges in the sample, is investigated in detail. Previous experimental results obtained with various picosecond and femtosecond light sources are successfully reproduced and the general resolution limits of solid-state photoemission using pulsed photon sources are explored. The results are potentially important for the design and interpretation of photoemission experiments with next-generation light sources, such as free-electron lasers and high-harmonic generation sources.

DOI: 10.1103/PhysRevB.79.035402 PACS number(s): 79.60.−i, 78.47.−p, 52.59.Sa

I. INTRODUCTION

Modern solid-state photoemission techniques comprise a powerful set of tools for determining the energy, momentum, dynamics, and to some extent also the spatial distribution of electron states in condensed matter. One prominent example is angle-resolved photoemission spectroscopy (ARPES), which is commonly applied to measure band structures, Fermi surfaces, and many-body effects, such as gaps and kinks in electronic band dispersions, with routine energy resolutions on the meV scale and momentum resolutions corresponding to less than 1% of typical Brillouin-zone dimensions.[1–3] Other examples are time-resolved photoemission spectroscopy (TRPES), which has opened up the possibility to measure the dynamics of nonequilibrium charge-carrier distributions on the femtosecond time scale,[4,5] and soft x-ray photoemission spectromicroscopy providing spatially resolved chemical information with submicrometer resolution.[6,7]

The evolution of these techniques has always been driven by improvements in instrumentation on the detector side as well as on the side of the light sources. But particularly the dramatic progress in the last decade is intimately connected with the advent of highly efficient electron spectrometers[8] and, more important for the following, with the availability of intense short-wavelength light sources. These are especially third-generation synchrotron-radiation sources delivering brilliant undulator radiation in the spectroscopically interesting extreme ultraviolet (UV) (EUV) to soft x-ray regime, on one hand, and ultrafast laser systems generating UV light pulses by upconversion techniques, on the other hand. Despite their extremely useful properties, when striving for the highest possible energy resolution in photoemission, both types of photon sources may imply a fundamental limit. Both are short pulsed (typically of picosecond or femtosecond time scale, respectively) and will therefore generate a relatively dense cloud of photoelectrons in front of the sample surface. On the way to the detector, the mutual Coulomb repulsion between the electrons will distort their initial energy and angle distributions and this space-charge distortion will in the end correspond to an effective loss of energy and angular resolution. Even for a typical synchrotron-radiation source, which delivers ~50 ps pulses of $\sim 10^4$ photons, space-charge effects in ARPES have recently been shown to bring about energy shifts and broadenings of ~10 meV,[9] whereas instrumental energy resolutions have now reached values of below 1 meV.[10]

The limitations of solid-state photoemission due to vacuum space-charge effects may become even more relevant in the near future, as the parameters of modern extreme ultraviolet and soft x-ray sources (in particular, pulse duration, number of photons per pulse, and spot size) are continuously pushed into new territory. Most notably, the recent development of high-harmonic generation[11,12] and free-electron laser sources[13] opens up intriguing possibilities in the field of femtosecond TRPES by extending the accessible binding-energy range into the core-level regime.[14–20] But the extremely high pulse densities of these other sources ($>10^7$ photons per pulse) can also lead to dramatic energy shifts and broadenings on the order of several eV,[21] thus obscuring any intrinsic spectroscopic signature.

The occurrence of such space-charge-induced spectral broadenings and shifts in electron emission from surfaces is by no means a new issue. There is a rather diverse literature on thermal electron emission,[22] photocathodes,[23,24] ultrafast electron diffraction,[25,26] photoemission microscopy,[27] and picosecond[9,28–38] and femtosecond[17,21,39,40] photoelectron spectroscopy. It is clear that space-charge effects in photoemission experiments with a pulsed photon source will critically depend on the parameters of the source: number of photons per pulse, spot size on the sample, pulse duration, and photon energy. However, for today's synchrotron and laser light sources these parameters may differ by orders of magnitude, so that via the material specific photoemission process each set of parameters will result in a distinct initial photoelectron distribution in real and momentum spaces. Although previous efforts have performed simple numerical simulations[9,38] or have used simple analytical models[21,34,37,40] with quite some success to explain space-

charge effects for a few typical experimental conditions, they have also yielded open questions related to, for instance, the exact functional dependence of the spectral broadening on the number of electrons per pulse, the role of mirror charges in the sample, the neglect of mutual Coulomb interaction in the photoelectron cloud in simulations, and the loss of angular resolution due to space-charge effects. In addition, previous studies do not fully clarify the validity range of the simple models, nor do they provide a few rough rules of thumb for the practitioner.

The goal of the present work is to explore the limits set by the vacuum space charge after pulsed photoemission from solid surfaces for experimental conditions as general and realistic as possible. The approach should therefore be global and *ab initio*. Accordingly, we set up a molecular-dynamics model which employs full N-body numerical simulations of the electron propagation from the surface to the detector (Sec. II). However, since the final spectral broadenings and shifts depend on many different photon source and material-specific parameters (exemplarily shown in Sec. III) and since it is *a priori* not clear whether our computational model is realistic, we will initially try to reproduce recent results from photoemission experiments with various pulsed picosecond and femtosecond ultraviolet and extreme ultraviolet sources (Sec. IV). After having proven the effectiveness of our approach, we will then perform simulations over wider parameter ranges, determine the functional dependence of space-charge effects on the most crucial parameters, and examine the ranges of validity of some simple analytical models (Sec. V). In the end, we are able to discuss some general implications of space-charge effects on today's and future photoemission experiments (Sec. VI).

II. COMPUTATIONAL MODEL

Figure 1 sketches a typical solid-state photoemission experiment with a pulsed photon source. Shortly after the incoming photon pulse has been absorbed in a certain volume near the surface of a solid sample, a cloud of photoelectrons is created in front of the surface. The phase-space distribution of the photoelectrons will depend on the parameters of the light pulse (number of photons per pulse, pulse duration, spot size, and photon energy) and on the material-dependent aspects of the photoemission process (quantum efficiency, kinetic-energy and emission-angle distributions).

In our numerical simulations, the photoelectron cloud containing a specified number of electrons is built up gradually. The electrons are started at discrete times during the photon pulse from a random position within the given spot size on the surface and with a random kinetic energy and a random emission angle taken from specified distributions. The temporal profile of the light pulse and the lateral profile of the illuminated surface area are assumed to be Gaussian with widths of τ_0 and d_0 [full width at half maximum (FWHM)], respectively. In the present work, the number of cloud electrons per pulse N_c ranges from 4 to $5\times10^6 e^-$ per pulse.

The propagation dynamics of the photoelectron cloud on its way to the detector is computed by performing self-consistent N-body numerical simulations. In each time step Δt, the new position and velocity of each electron are determined from the present position and velocity and the net Coulomb force on the electron using leap-frog integration. For the force calculation, the hierarchical tree-code method is employed, which is reasonably accurate and requires only $\mathcal{O}(N \log N)$ operations.[41,42] The charge distribution is first partitioned into a tree structure that represents a recursive subdivision of space into smaller and smaller cubic cells with, in the end, at most one electron in them. Then, to calculate the total force on any electron, the tree structure is traversed starting at the root cell, which contains the entire electron cloud, and going to ever finer spatial structures. In the process, the current cell is treated in two possible ways, depending on an "opening angle" defined as the ratio of the width of the cell to the distance between its center of mass and the electron for which the force is calculated. If the opening angle is smaller than a fixed accuracy parameter θ,

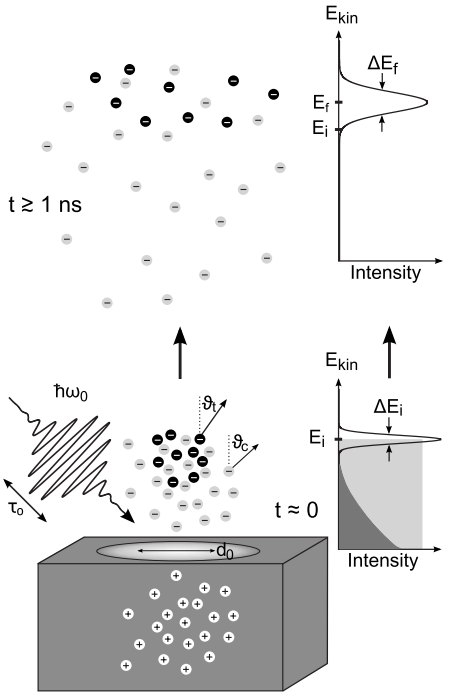

FIG. 1. Schematic of a solid-state photoemission experiment employing a pulsed photon source. A light pulse with energy $\hbar\omega_0$ and duration τ_0 impinges on a surface area of characteristic width d_0 and kicks out photoelectrons. In the numerical simulation, the photoelectrons are divided into cloud electrons (gray dots) and test electrons (black dots), both having specified initial kinetic energy (E_{kin}) and emission angle (ϑ_c, ϑ_t) distributions depending on the source parameters and sample properties. For the test electrons, a sharp Gaussian energy distribution (mean position E_i and width ΔE_i) is typically selected. The gray energy areas in the energy spectrum depict simple energy distributions for the cloud electrons. Positive mirror charges in the bulk of the sample (white dots) are generally included in the simulation. The propagation of the electrons toward the detector is influenced by mutual Coulomb interaction. After about 1 ns, when the total Coulomb energy has become negligible, the final energy spectrum of the test electrons is obtained. In general, it will be shifted and broadened with respect to the original spectrum ($E_f \neq E_i, \Delta E_f > \Delta E_i$).

the partial force due to the cluster of electrons in the cell is approximated by the force due to a point charge at the cluster's center of mass. Otherwise, the current cell is resolved into its subcells which are examined in the same way. If necessary, this process continues until forces from individual electrons are added to the total force being accumulated.

In a typical simulation run, it roughly takes a few nanoseconds (depending on the mean electron velocity and the initial electron density) until the total Coulomb energy of the photoelectron cloud becomes negligible. The run is then stopped and the final kinetic-energy and momentum distributions are obtained. With a typical time step $\Delta t < 20$ ps and a force accuracy parameter $\theta = 1$, the total energy is generally conserved to $<0.1\%$.

The whole procedure—random generation and self-consistent propagation of the electron cloud—is repeated a few times for a given parameter set. However, to get significantly better statistics in the energy and momentum ranges of interest, we introduce the so-called test electrons in the simulation (see Fig. 1). These "virtual" electrons, typically about 10^4 in each run, feel the space-charge cloud but they do not contribute to it; they are generated in the same way as the "real" cloud electrons, except that they start with very narrow (usually Gaussian) energy and angle distributions.

When using the described scheme, in remarkably many cases, the final test electron energy distribution can reasonably be fitted to a Gaussian. Then, the space-charge-induced shift and broadening are calculated via $\Delta E_{\text{shift}} = E_f - E_i$ and $\Delta E_{\text{broad}} = \sqrt{(\Delta E_f)^2 - (\Delta E_i)^2}$, where E_i and E_f are the initial and final mean energies of the test electron energy distribution and ΔE_i and ΔE_f are the initial and final FWHM widths (see Fig. 1). In cases where the resulting energy distribution deviates significantly from a Gaussian, the mean and variance calculated directly from the distribution are used as a measure of the shift and broadening, respectively. Examples for such non-Gaussian energy distributions will be given in Sec. III. In general, there will be also some electrons in the distribution, which are shifted by a multiple of the final FWHM as a consequence of short-range scattering between electrons. These events are, however, rare—typically less than 0.1% of the electrons are affected—so that the resulting long flat tails toward higher energies do not disturb the overall distribution too much. Altogether, we assign an error of $\sim 10\%$ to the computed values of E_f and ΔE_f.

Finally, the presence of a sample with a surface at $z=0$ is taken into account in two different ways. First, during the simulation the surface acts as an absorber of all electrons entering the sample half space $z<0$. These electrons are henceforward ignored in the simulation run. Second, the surface is treated as perfectly metallic and, therefore, as an equipotential surface. To emulate this case, each cloud electron in the vacuum at (x,y,z) with $z>0$ is instantaneously accompanied by a positive mirror charge inside the sample at $(x,y,-z)$ (see Fig. 1). The resulting cloud of mirror charges exerts attractive Coulomb forces on both the test and the cloud electrons and may significantly influence the calculated energy shifts and broadenings.[9] The other extreme, a nonconducting sample, in which stationary photohole states are left behind after the photoemission process, is not considered in the present work.

III. RELEVANT PARAMETERS

Space-charge-induced spectral broadenings and shifts depend on the initial density of the photoelectron cloud in phase space, which in turn depends on source and sample-specific parameters of the photoemission experiment. To warm up, some qualitative statements about the most relevant parameters will be given in this section illustrated by variations of an example that may be considered representative for valence-band photoemission of a metallic surface with short pulsed vacuum-ultraviolet light: a circular light spot with a diameter of $d_0 = 200$ μm, a pulse duration of $\tau_0 = 50$ fs, $N_c = 10^4$ cloud electrons per pulse, an initial test electron energy of $E_i = 30$ eV (Gaussian distribution with 50 meV FWHM), normal emission of the test electrons ($\vartheta_t = 0°$), a rectangular energy distribution of the cloud electrons in the interval of 0–30 eV, an angular distribution corresponding to isotropic emission, and mirror charges present in the sample. The calculated initial and final energy distribution curves of the test electrons are shown in Figs. 2(a) and 2(b), respectively.

A. Number of electrons per pulse

It is expected that the higher the number of (cloud) electrons per pulse N_c the stronger are the spectral distortions. Quantitative predictions are, however, difficult. Only recently, it has become clear that non-negligible space-charge effects occur already at rather low values of N_c of about $1000e^-$ per pulse.[9] Also, the N_c dependence of the energy broadening is still puzzling. Femtosecond ultraviolet photoemission results suggest a $\sqrt{N_c}$ dependence,[40] whereas photoemission experiments with a picosecond extreme ultraviolet source conform more to a linear dependence.[9] The systematic studies of the N_c dependence of energy broadenings and shifts, following in Secs. IV and V, will help to clarify these issues.

B. Pulse duration and spot size

Immediately after the photoemission process, the average distance between cloud electrons is determined by the pulse duration τ_0 and the source size d_0, which set the characteristic length scales in the directions perpendicular and parallel to the surface, respectively. The velocity of an electron with a kinetic energy of 30 eV is $v_0 \approx 3.2$ mm/ns. So, if $\tau_0 \ll d_0/v_0$ (62 ps in the present case) all electrons will reside in a quasi-two-dimensional disk in front of the surface. In this short pulse limit, the average distance between electrons is given by $d_0/\sqrt{N_c}$, independent of τ_0. Thus, the energy broadening is expected to be almost independent of the pulse duration [cf. Fig. 2(e) ($\tau_0 = 50$ ps) and Fig. 2(b) ($\tau_0 = 50$ fs)] and strongly dependent on the spot diameter [cf. Fig. 2(i) ($d_0 = 200$ μm) and Fig. 2(m) ($d_0 = 50$ μm)]. The other limiting case occurs when $\tau_0 \gg d_0/v_0$. Then, the average electron distance is proportional to τ_0/N_c and the energy broadening is expected to be independent of d_0. As to the different types of light sources, ultrafast laser systems usually fall in the first category, whereas synchrotron light sources lie somewhere in between the limiting cases. The long-pulse limit, realized by

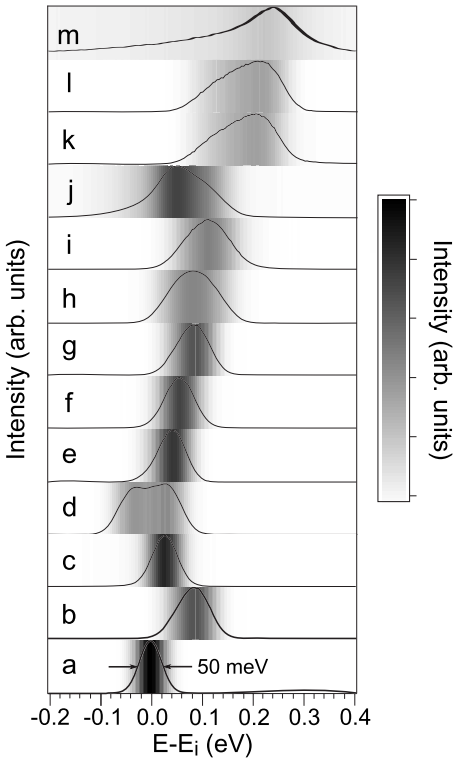

FIG. 2. Influence of various simulation parameters on a Gaussian test electron spectrum with mean position $E_i=30$ eV and $\Delta E_i=50$ meV FWHM [spectrum (a)]. The basic parameters of the numerical simulation, leading to spectrum (b), are number of cloud electrons per pulse $N_c=10^4$, spot size diameter $d_0=200$ μm, pulse duration $\tau_0=50$ fs, homogeneous energy and isotropic emission-angle distribution of the cloud electrons ($E_c=0-30$ eV, $\vartheta_c=0°-90°$), normal test electron emission ($\vartheta_t=0°$), mutual Coulomb interactions between cloud electrons, and interactions with mirror charges included. Changing individual parameters results in the following spectra: (c) $E_i=15$ eV; (d) $\tau_0=200$ ps, and $N_c=2\times10^4$; (e) $\tau_0=50$ ps; (f) $\vartheta_t=45°$; (g) no Coulomb interaction between cloud electrons; (h)–(j) Gaussian cloud electron spectra with 50 meV FWHM and mean energies of 1, 30, and 900 eV; (k) no mirror charges; (l) $\vartheta_c=0°-45°$; and (m) $d_0=50$ μm and Gaussian cloud electron spectrum with 50 meV FWHM and mean energy 30 eV.

quasicontinuous light sources, will not be investigated in this paper. Figure 2(d) ($\tau_0=200$ ps) just serves as an example for an energy distribution that can emerge when the length of the initial electron cloud is larger than its diameter.

C. Kinetic-energy distribution

Generally, when the energies of the test and cloud electrons are similar, the test electrons will spend a longer time close to a large number of interaction partners. Hence, the energy broadening and shift are larger for a narrow energy distribution of the cloud electrons that is centered near the mean test electron energy [cf. Fig. 2(i) (narrow distribution) and Fig. 2(f) (wide distribution)]. On the other hand, for wide energy distributions of the cloud electrons, space-charge-induced broadenings and shifts are slightly more pronounced for test electron energies near the maximum cloud electron energy [cf. Fig. 2(c) ($E_i=15$ eV) and Fig. 2(f) ($E_i=30$ eV); $E_c=0-30$ eV]. In that case, the test electrons have the entire cloud in their back and are pushed to higher energies for the longest possible time. As to the dependence of space-charge effects on the mean electron energy, Fig. 2(h) ($E_i=1$ eV), Fig. 2(i) ($E_i=30$ eV), and Fig. 2(j) ($E_i=900$ eV) suggest that this dependence is not too pronounced if one considers that in these figures the mean energy has been varied by almost 3 orders of magnitude.

D. Emission-angle distribution

Arguments, similar to those just made, hold for the initial angular distributions of test and cloud electrons. The higher the concentration of cloud electrons the test electron is seeing, the stronger will be the space-charge effects. Thus, a forward focusing of the cloud electrons strongly increases the energy broadening and shift of the test electrons [Fig. 2(l) ($\vartheta_c=0°-45°$)], whereas an off-normal test electron emission leads to a smaller shift [Fig. 2(f) ($\vartheta_t=45°$)] if the cloud electrons are emitted isotropically. In general, the emission-angle distribution is one of the more important factors governing space-charge effects. But, unfortunately, it is also a parameter that is hard to measure completely.

E. Mirror charges

As pointed out in Ref. 9, changes in the charge distribution inside the sample can significantly modify the final test electron energy, depending on the location of the test electron relative to the majority of the cloud electrons. For a test electron that is behind the cloud, the positive charge in the sample will act in conjunction with the cloud electrons and slow down the test electron even further. In the other case, when the test electron is ahead of the cloud electrons, the interactions counteract each other and the acceleration of the test electron away from the cloud will become smaller. In both cases, the test electron energy is reduced. The importance of mirror-charge effects is illustrated by Fig. 2(k), where the mirror charges in the sample have been switched off. The spectrum is strongly shifted and asymmetric. This example demonstrates that mirror charges can in fact partly compensate space-charge effects.

F. Coulomb interaction between cloud electrons

For the rather small number of cloud electrons per pulse considered here, switching off the mutual interaction between them has no significant effect [Fig. 2(g)]. This justifies the simple numerical approach taken in Ref. 9, where the cloud electrons have been assumed to move on straight lines. For higher N_c or when $\Delta E_{\text{broad}} \approx E_i$, however, this approximation is no longer legitimate.

In conclusion, the major lesson from the above considerations on a simple example appears to be that there are many different factors governing space-charge effects in solid-state photoemisison and, consequently, that there is no substitute for realistic microscopic simulations if one wants to understand a specific experimental situation quantitatively.

IV. COMPARISON WITH EXPERIMENTS

The pursuit of the ultimate resolution and the availability of other sources has recently led to renewed interest in space-charge effects in solid-state photoemission.[9,21,40] In this section, we validate our numerical approach on recent experimental results obtained with a third-generation synchrotron light source,[9] an ultrafast laser system,[40] and a free-electron laser.[21] For these selected experiments, the parameter ranges as well as the observed space-charge effects span several orders of magnitude.

A. 60 ps EUV synchrotron-radiation source

With the recent comprehensive study by Zhou *et al.*,[9] space-charge effects, largely ignored as a possible resolution limiting factor in ARPES in the past, were suddenly back on the agenda. In this work, the authors have studied space- and mirror-charge effects in high-resolution ARPES using a third-generation synchrotron light source (the ALS in Berkeley). To probe the spectral distortions, they used the Fermi edge of a polycrystalline gold sample kept at a temperature of 20 K. Excitation with a photon energy of $h\nu=34$ eV then resulted in an energy distribution like the one shown in Fig. 3(a), with a sharp Fermi cutoff at $E_i=29.38$ eV. The photon pulses used in the experiment had a duration of 60 ps FWHM and the spot size on the sample was about 0.43×0.3 mm^2 FWHM. The number of (cloud) electrons per pulse reached values up to 2000 and the (test) electrons were detected at an emission angle of $\vartheta_t=45°$.

Using these parameters and assuming a cosine angular distribution of the cloud electrons, we have computed the energy shift and broadening of the Fermi edge as a function of N_c, the number of cloud electrons per pulse. In the simulations, the test electrons had a Gaussian energy distribution centered on $E_i=29.38$ eV with a width of $\Delta E=18$ meV FWHM. Figure 3(b) compares the results of our simulations with the experimental results obtained by Zhou *et al.*[9] The nearly linear N_c dependence of both the shift and the broadening and the fact that the shift is smaller than the broadening are reproduced very well. The latter can be traced back to the off-normal-emission geometry. For normal emission of the test electrons, the energy shift becomes larger than the broadening. Although experimental and simulated results differ by a factor of 2 [note the different scales of the vertical axes in Fig. 3(b)], this does not necessarily depreciate the value of the computational model. The absolute energy values are small and the experimental results can in fact be reproduced almost exactly when a smaller spot size or a more forwardly directed emission pattern is used in the simulation.

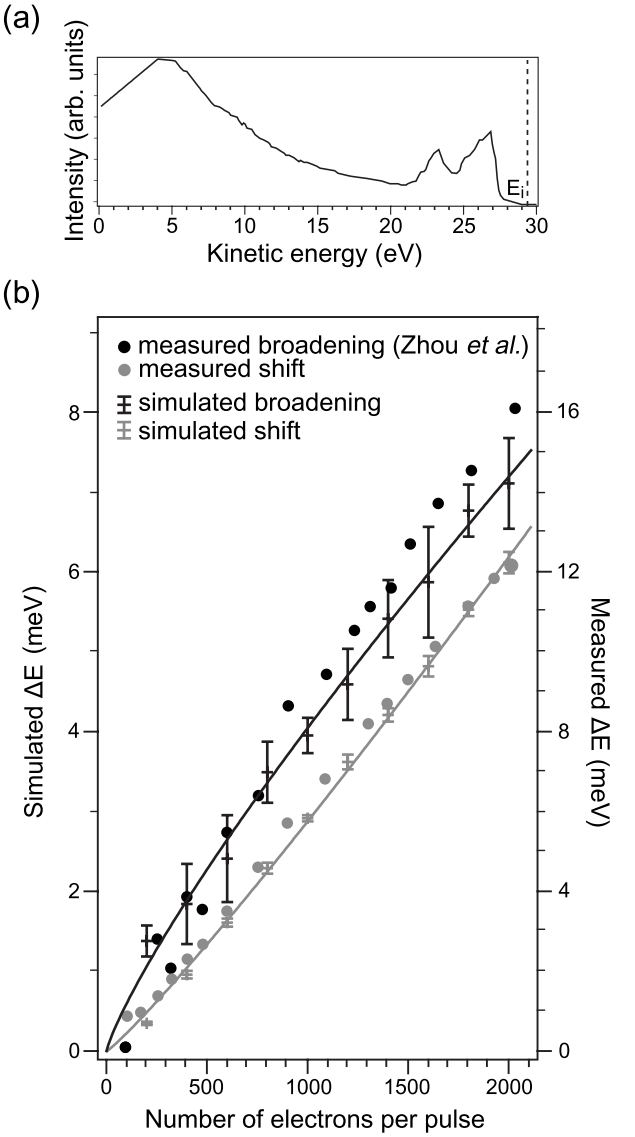

FIG. 3. Space-charge effects on the photoemission spectrum of a polycrystalline gold sample under irradiation with $\tau_0=60$ ps, $\hbar\omega_0=34$ eV photon pulses. (a) Typical energy distribution curve with the Fermi cutoff at 29.38 eV (taken from Ref. 9). (b) Comparison between simulated and measured (Ref. 9) Fermi edge shifts and broadenings in the range of $(0-2000)e^-$ per pulse. Note the different scales of the vertical axes. Power-law fits to the simulated energy shift and broadening serve as guides for the eyes ($\Delta E_{\text{shift}}\propto N_c^{1.11}, \Delta E_{\text{broad}}\propto N_c^{0.83}$). The spot size is 0.43×0.3 mm^2 and the test electrons are emitted with an angle of 45°. In the simulation, a cosine distribution of the cloud electron emission angles is used.

B. 40 fs UV laser source

Inspired by the work of Zhou *et al.*,[9] Passlack *et al.*[40] subsequently investigated space-charge effects in photoemission with a femtosecond optical laser system. They used the Shockley surface state of the Cu(111) surface as a sharp spectral feature and probed its energetic broadening in intensity dependent two-photon-photoemission experiments with 40 fs 3.1 eV photon pulses. Figure 4(a) shows a typical spectrum acquired at normal emission. The kinetic energy of the surface-state peak is naturally rather low: 0.912 eV. The spot size in the experiments was about 1.15×0.9 mm^2 FWHM.

In the numerical simulations, the major source of uncertainty was the incorporation of the energy-momentum relationship of the surface-state band, which causes the photoemission peak to disperse as a function of emission angle [see Fig. 4(a)]. Since the full angular distribution was not

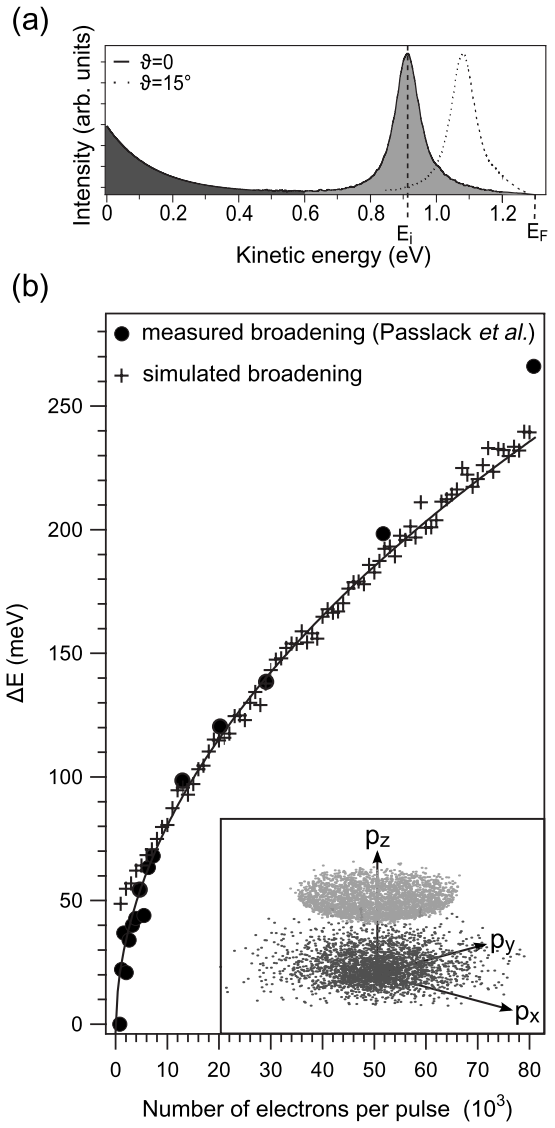

FIG. 4. Space-charge effect on the two-photon-photoemission spectrum of a Cu(111) surface under irradiation with intense $\tau_0 = 40$ fs, $\hbar\omega_0 = 3.1$ eV photon pulses. (a) Typical energy distribution curves of the Shockley surface state for emission angles of $\vartheta_t = 0°$ (solid curve) and $\vartheta_t = 15°$ (dotted curve), respectively (taken from Ref. 40). In the case of normal emission, the surface-state photoemission peak (light gray) is located at a kinetic energy of 0.912 eV and sits on a characteristic secondary electron background (dark gray). (b) Comparison between the simulated and measured (Ref. 40) energy broadenings of the surface-state peak in the range of $(0-80\,000)e^-$ per pulse. The simulated broadening shows a power-law behavior $\Delta E_{\mathrm{broad}} \propto N_c^{0.5}$ (solid line). The spot size is 1.15×0.9 mm^2 and the test electrons are emitted in the normal direction. In the simulation, an angular distribution of the cloud electrons is assumed that accounts for the parabolic energy-momentum dispersion relation. The inset illustrates the distribution of surface-state (light gray) and secondary electrons (dark gray) in momentum space.

measured in the experiment, a few assumptions had to be made in the numerical simulations. The secondary electron background, as determined from the normal-emission spectrum in Fig. 4(a), was assumed to be constant over the emission hemisphere, the energy–wave-vector relation $E(k_\parallel)$ of the surface state was taken to be parabolic with an effective mass of $0.41 m_e$,[43] and photoemission intensity variations due to matrix-element effects were neglected. A representative electron distribution in momentum space is illustrated in the inset in Fig. 4(b). The surface-state electrons in light gray are well separated from the secondary electrons in darker gray. Their number ratio critically affects the calculated energy broadening. The best agreement between experiment and simulation is obtained for a ratio of surface-state to secondary electrons of about 0.5.

Simulated and measured[40] energy broadenings of the normal-emission surface-state peak are compared in Fig. 4(b). The agreement is excellent over almost the entire range of $(0-80\,000)e^-$ per pulse. Only for the lowest and the highest electron numbers some small deviations occur. The simulated energy broadening can be well approximated by a power law $\Delta E_{\mathrm{broad}} \propto N_c^x$ with $x \approx 0.5$. As will be further discussed in Sec. V, this square-root behavior is characteristic for photoelectron pulses with very low kinetic energies (≤ 1 eV) and may not be extrapolated to higher energies.

In addition to the energy broadening effects, the results of our simulations suggest a stretching of the surface-state dispersion relation $E(k_\parallel)$ due to space-charge effects. In the present case, off-normally emitted surface-state electrons have higher kinetic energies as compared to normally emitted surface-state electrons, so that the first will be ahead of the latter. As a consequence, the surface-state electrons with the largest emission angles and thus the largest wave vectors parallel to the surface $k_\parallel$ will be pushed to higher kinetic energies, whereas the electrons at the bottom of the band, at $k_\parallel = 0$, will be slowed down. For the normal-emission peak ($k_\parallel = 0$), the numerical simulations reveal an energy shift of about -1.5 μeV per cloud electron. The experimental study, on the other hand, reports a negligible energy shift up to $N_c \approx 40\,000$.[40] However, since the simulated energy shift critically depends on the densities of surface-state and secondary electrons in momentum space [inset of Fig. 4(b)], it is expected that this discrepancy can be overcome once a better knowledge of the angular distribution of both types of photoelectrons is available.

C. 40 fs EUV free-electron laser

With the availability of a free-electron laser in the extreme ultraviolet regime (FLASH in Hamburg), femtosecond time-resolved core-level photoemission spectroscopy has now come within reach. Pietzsch *et al.*[21] recently performed such measurements on the W $4f$ lines with laser pulses of 118.5 eV photon energy and a duration of about 40 fs and they particularly studied the space-charge-induced spectral distortions as a function of the pulse intensity. A typical spectrum for a low pulse intensity is plotted in Fig. 5(a). The number of photons per pulse was determined using a multichannel-plate-based diagnostic tool.[44] The number of photoelectrons per pulse, however, was not measured independently; it was calculated from the number of photons using tabulated values for the photoionization cross section, the photon penetration depth, and the electron escape depth.

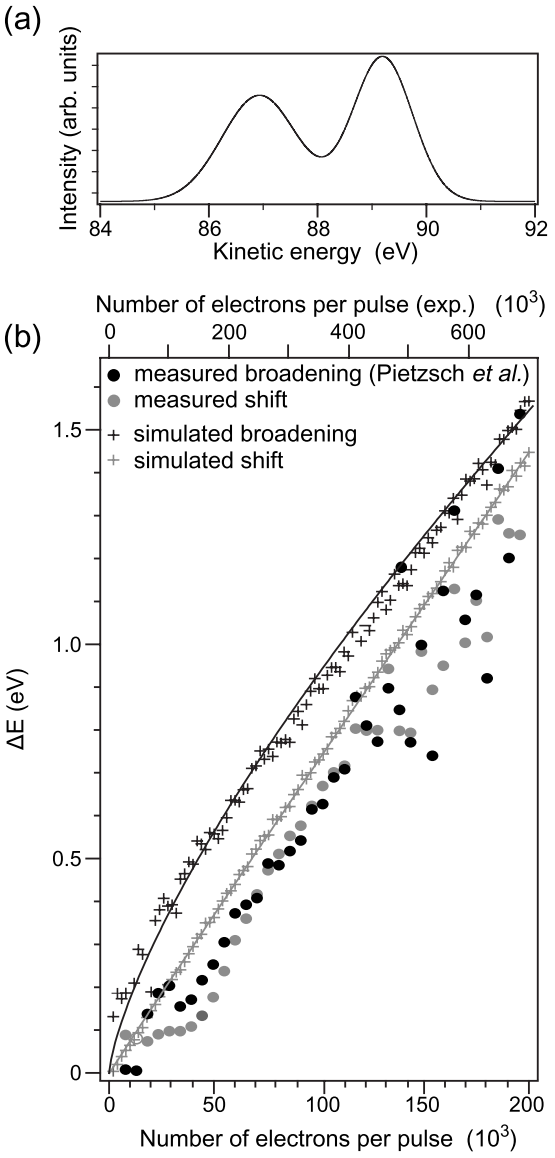

FIG. 5. Space-charge effects on a W $4f$ core-level spectrum under irradiation with τ_0=40 fs, $\hbar\omega_0$=118.5 eV photon pulses. (a) Typical energy distribution curve with photoemission peaks at kinetic energies of ~87 and ~89 eV (taken from Ref. 21). (b) Comparison between simulated and measured (Ref. 21) peak shifts and broadenings in the range of (0–200 000)e^- per pulse. Note the different scales of the axes for the simulated (bottom axis) and measured data (top axis). Power-law fits to the simulated energy shift and broadening serve as guides for the eyes ($\Delta E_{\text{shift}} \propto N_c^{0.98}$, $\Delta E_{\text{broad}} \propto N_c^{0.73}$). The spot size is 0.27×0.4 mm^2. In the simulation, a cosine distribution of the cloud electron emission angles is used and the test electron acceptance angle is set to 13°.

The experiments were performed with a spot size of about 0.27×0.4 mm^2.

In the numerical simulations, we have assumed a cosine angular distribution of the cloud electrons and set the test electron acceptance angle to 13°, in accordance with the photoemission experiment. Figure 3(b) compares the results of our simulations to the experimental results of Pietzsch *et al.*[21] The plotted energy shifts and broadenings represent average values for the two W $4f$ peaks in the spectrum. The linear energy shift and the nearly linear energy broadening as functions of the number of electrons per pulse are again well reproduced by the simulations. The simulated results, however, overestimate the experimentally determined values by about a factor of 3 [note the different scales of the horizontal axes in Fig. 5(b)]. This rather large deviation may presumably arise from an error in the experimentally determined electron numbers, considering the fact that these numbers are obtained very indirectly.[21]

The major conclusion to be drawn from the examples presented above then is that the computational model used to simulate the space-charge effects is fairly realistic. The measured dependencies of energy broadenings and shifts on the number of electrons per pulse are qualitatively well reproduced for all discussed cases. Quantitative deviations lie within a factor of 3 and are likely due to uncertainties in the experimental parameters. The angular distribution of the photoelectrons and the number of electrons per pulse, in particular, are critical parameters that are often not fully determined in the experiments or sometimes hard to measure accurately. For experiments tainted with such uncertain parameters, the numerical simulations may provide a much better understanding of the observed space-charge effects.

V. GENERAL LIMITS

The rather successful modeling of the experimental results, as just shown, suggests using the numerical simulations to fill the parameter gaps between the specific experimental situations discussed in Sec. VI. The goal of this section thus is to explore the resolution limits posed by the Coulomb interaction between the emitted electrons on a more general basis. To this end, we will first allude to two simple analytical models and will then discuss two branches of photoemission spectroscopy, which reflect two rather different situations in terms of the kinetic-energy distribution and the pertinent energy scale. In core-level spectroscopy, most of the photoelectrons are concentrated in a narrow energy interval and the relevant energy scale is roughly 0.1 eV. In valence-band spectroscopy, on the other hand, the feature of interest—for example, a Fermi edge—usually sits on a wide energy background containing almost all of the emitted electrons. Here the interesting energy scale is usually smaller than 10 meV. In addition, space-charge-induced distortions of the angular distribution may become relevant, as they will lead to a loss of momentum resolution.

A. Simple models for the energy broadening

In the literature, two very simple analytical models have been used to estimate the onset of space-charge effects in pulsed photoemission spectra and, in particular, to explain the experimentally observed dependencies of the energy broadening on the number of electrons per pulse N_c, the spot size diameter d_0, and the initial kinetic energy E_i.

The first model was put forward by Long *et al.*[37] The sample is assumed to be a sphere of diameter d_0 and the photoelectrons are assumed to reside within an expanding spherical shell of negligible thickness, implying that the

pulse duration is much smaller than the transit time of the fastest electrons to the detector. For the energy spread, in this case the difference between the energy gained by an electron at the leading edge and the energy lost by an electron at the trailing edge of the shell, the authors find that

$$\Delta E_{\text{broad}} \approx 6 \times 10^{-6} \frac{N_c}{d_0}, \tag{1}$$

where ΔE_{broad} is given in eV and d_0 is in millimeter. Relation (1) predicts that the energy broadening in pulsed photoemission spectra is independent of the electron energy and the pulse duration, which is consistent with the considerations on the short pulse limit in Sec. III. Note that, coincidentally, Eq. (1) corresponds to the potential energy of an electron that sits either at the center of a uniformly charged disk or on the surface of a charged sphere, both with a total charge $-N_c e$ and diameter d_0. Hence, the same estimate for the onset of Coulomb energy broadening could be obtained even more easily by employing simple electrostatic models for the electron cloud and arguments based on energy conservation.[34]

The second model has originally been developed to describe the propagation dynamics of femtosecond electron packets in ultrafast electron diffraction[25] but was later also used to explain the space-charge-induced broadening in femtosecond pulsed photoemission spectra.[40] The charge distribution is assumed to be pancake shaped, i.e., the ratio of the spatial length of the electron cloud to its diameter is very small, and the space-charge-induced energy spread is assumed to be proportional to the group velocity of the electron pulse and to the rate of broadening of the pulse length. The latter is calculated from analytical formulas for the potential of a homogeneously charged disk. It is found that

$$\Delta E_{\text{broad}} \approx C \sqrt{\frac{N_c E_i}{d_0}}, \tag{2}$$

where ΔE_{broad} and E_i are given in eV, d_0 is in millimeter, and the factor C is somewhere in the range of 0.002–0.005.[25,40] Contrary to relation (1), this "mean-field model"[25] of femtosecond electron pulse propagation predicts a square-root dependence on the number of electrons per pulse and spot diameter and, additionally, a square-root dependence on the mean kinetic energy. In what follows, the predictive power and range of validity of both models will be investigated within the range of parameters typically used in core-level and valence-band photoemission spectroscopies.

B. Core-level spectroscopy

We regard the following simplified scenario as characteristic of core-level photoemission spectroscopy [generally known as x-ray photoelectron spectroscopy (XPS) or electron spectroscopy for chemical analysis (ESCA)]: a single Gaussian peak centered on the variable energy E_i and with a constant width of 100 meV (FWHM) representing the initial kinetic-energy distribution of both the cloud and the test electrons. The angular distribution is assumed to be equally simple: isotropic emission of the cloud electrons and surface-normal emission of the test electrons. In the numerical simulations then the number of cloud electrons per pulse N_c, the diameter of the light spot d_0, the initial mean energy E_i, and the pulse duration τ_0 are varied systematically as follows: $N_c = 100-500\,000$, $d_0 \in \{0.1, 0.4, 1 \text{ mm}\}$, $E_i \in \{1, 10, 100, 1000 \text{ eV}\}$, and $\tau_0 \in \{20 \text{ fs}, 1 \text{ ps}, 50 \text{ ps}\}$. Note that unusually low values of the kinetic energy have been included because sometimes a valence-band spectrum taken with a low photon energy can resemble a core-level spectrum, as for example in the second case discussed in Sec. IV.

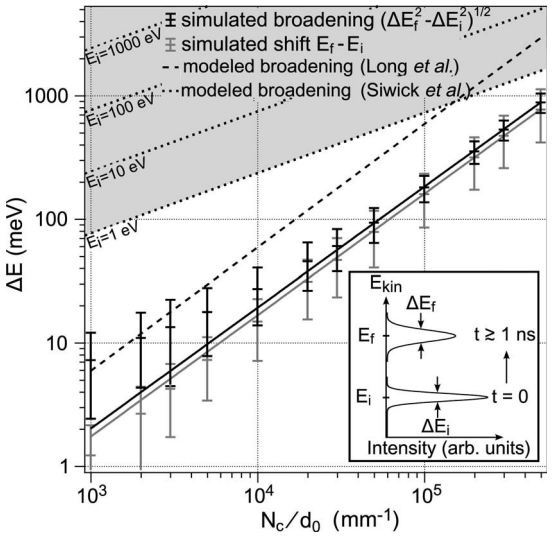

FIG. 6. Simulated energy shift (gray data points) and energy broadening (black data points) as functions of the cloud electron density N_c/d_0 for a situation similar to core-level photoemission spectroscopy. The error bars result from a systematic variation of the light spot diameter d_0 (0.1, 0.4, and 1 mm), mean energy E_i (1, 10, 100, and 1000 eV), and pulse duration τ_0 (20 fs, 1 ps, and 50 ps). In the simulation, identical initial Gaussian energy distributions for cloud and test electrons with 100 meV FWHM are used. The cloud electrons are emitted isotropically over the hemisphere; the test electrons are emitted in the normal direction. The solid lines represent power-law fits to the simulated data [$\Delta E_{\text{shift}} \propto (\frac{N_c}{d_0})^{0.98}, \Delta E_{\text{broad}} \propto (\frac{N_c}{d_0})^{0.98}$]. The dashed line corresponds to relation (1) (Ref. 37); the dotted lines plotted over the area highlighted in gray are calculated from relation (2) for the different mean energies E_i (Refs. 25 and 40). The inset illustrates the space-charge effects on an energy spectrum.

Figure 6 shows the calculated energy shift and broadening of the test electron spectrum as functions of the linear electron density N_c/d_0. The error bars result from the systematic variation of the parameters; they represent the standard deviations. We note that in the case of long pulses ($\tau_0 = 50$ ps) the energy shift tends to zero and mostly lies outside the given error bars [see also Fig. 2(c) for a typical line shape in the long pulse limit]. As indicated by the fitted solid lines, the energy shift as well as the energy broadening approach a linear dependence on N_c/d_0 at high electron densities. In this regime, relation (1), the model proposed by Long *et al.*,[37] overestimates the simulated space-charge-induced energy broadening by a factor of 3. At low electron densities ($N_c/d_0 < 10^4 e^-/\text{mm}$), the energy broadening deviates from the linear relationship and approaches some finite value of ~ 10 meV. This behavior is connected with how the broad-

ening is being determined (see inset of Fig. 6). Considering that the initial peak width is 100 meV, the accuracy of the simulations is simply not sufficient to reproduce the linear dependence down to the lowest electron densities.

The linear dependence on N_c/d_0 can be rationalized straightforwardly. Space-charge-induced energy broadening generally results from the conversion of Coulomb potential energy of the suddenly created electron cloud into kinetic energy as the cloud propagates to the detector. Since the electron cloud in pulsed photoemission experiments is typically pancake shaped and the potential energy per electron in such a charge distribution is proportional to N_c/d_0, it follows that the initial potential-energy spread and thus also the final kinetic-energy spread will be proportional to N_c/d_0.

The dotted lines on the gray area in Fig. 6 represent the energy broadening predicted by relation (2), the mean-field model of electron pulse propagation in ultrafast electron diffraction.[25,40] Clearly, this model does not describe the situation adequately. It overestimates the space-charge effects in the studied parameter range and suggests a strong energy dependence as well as a square-root dependence on N_c/d_0, both not existing in the data set.

As to core-level photoemission spectroscopy in general, Fig. 6 gives a quantitative estimate for the onset of space-charge broadening in the spectra. For the space-charge-induced energy broadening to be kept below ~50 meV, a value comparable to the rather moderate energy resolution typically used, linear pulse densities must be limited to fewer than 10 000e^-/(pulse mm). This number agrees within a factor of 2 with experimentally determined onsets of space-charge broadening,[28,29,37] in particular with the results of the second study[40] discussed in Sec. IV [see Fig. 4(b)].

C. Valence-band spectroscopy

In high-resolution angle-resolved photoemission spectroscopy (ARPES), an important focus usually lies on fine details of the valence-band structure near the Fermi energy. To simulate a representative case, we employ a rectangular energy distribution of the cloud electrons extending from 0 to E_i, the initial energy of the test electrons. Hence, this scenario emulates the broadening of a Fermi edge when the secondary electron background and the valence band show relatively little structure. As in the simulations of the core-level case, the cloud electron emission is isotropic and the test electrons are emitted in the forward direction. The number of cloud electrons per pulse N_c, the spot diameter d_0, the mean energy E_i, and the pulse duration τ_0 are again varied in the simulations as follows: N_c=4–40 000, $d_0 \in \{0.04, 0.1, 0.4 \text{ mm}\}$, $E_i \in \{1, 10, 100 \text{ eV}\}$, and $\tau_0 \in \{10 \text{ fs}, 10 \text{ ps}\}$.

Figure 7(a) displays the resulting energy shift and broadening of the test electron spectrum as functions of the linear electron density N_c/d_0. Although for a given value of N_c/d_0 the shifts and broadenings vary on average by a factor of about 2 [see error bars in Fig. 7(a)], general trends are again clearly discernible [solid lines in Fig. 7(a)]. For $N_c/d_0 > 1000e^-$/mm, a linear dependence of the energy shift and broadening on N_c/d_0 can be identified, whereas at lower

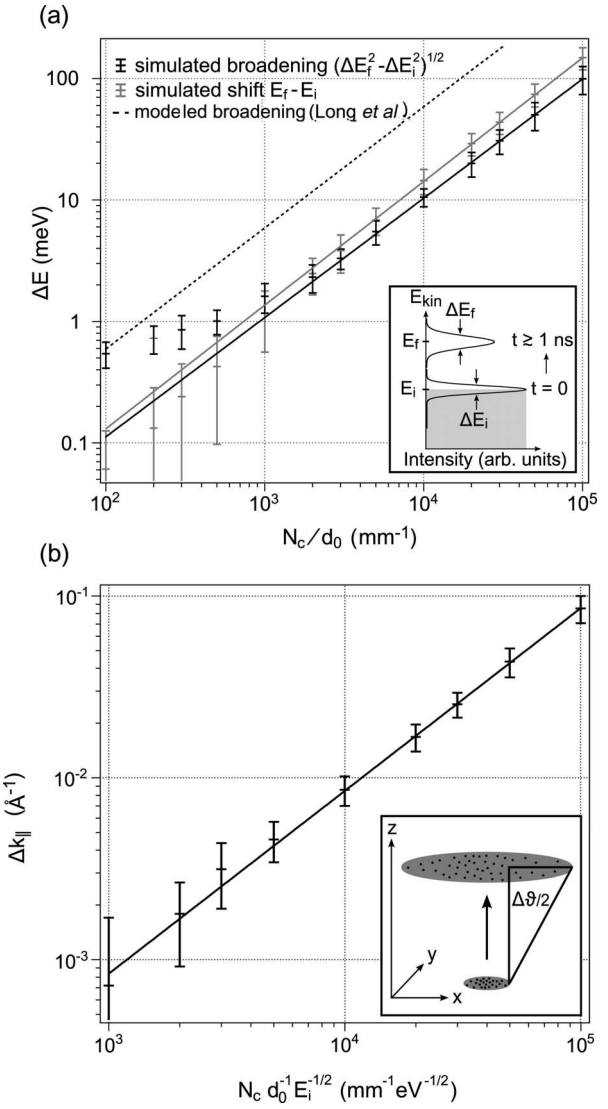

FIG. 7. (a) Simulated energy shift (gray data points) and energy broadening (black data points) as functions of the cloud electron density N_c/d_0 for a situation corresponding to angle-resolved valence-band spectroscopy. The error bars result from a systematic variation of the light spot diameter d_0 (0.04, 0.1, and 0.4 mm), mean energy E_i (1, 10, and 100 eV), and pulse duration τ_0 (10 fs and 10 ps). In the simulation, an initial Gaussian test electron energy spectrum with mean energy E_i and 5 meV FWHM is used sitting on top of a rectangular distribution of the cloud electron energies in the interval $0-E_i$ (see inset). The cloud electrons are emitted isotropically over the hemisphere; the test electrons are emitted in the normal direction. The solid lines represent power-law fits to the simulated data $[\Delta E_{\text{shift}} \propto (\frac{N_c}{d_0})^{1.02}, \Delta E_{\text{broad}} \propto (\frac{N_c}{d_0})^{0.98}]$. The dashed line corresponds to relation (1) (Ref. 37). (b) Simulated momentum broadening as a function of $N_c/(d_0\sqrt{E_i})$. The same parameter sets as in (a) are used, except that the mean energies E_i are now 1, 25, and 100 eV. The inset illustrates the space-charge-induced divergence of the electron distribution in real space.

electron densities the determination of the shift becomes rather inaccurate and the broadening tends to saturate at some finite value well below the width of the initial energy distribution of the test electrons (5 meV FWHM). In the

linear regime, the model proposed by Long *et al.*[37] overestimates the onset of space-charge effects [solid lines in Fig. 7(a)], which is understandable because the model is based on the assumption of a near monoenergetic energy distribution. The energy broadening predicted by the mean field model of ultrafast electron diffraction[25] has not been included in this figure because, as shown above, it strongly overestimates the energy dependence of space-charge effects.

Regarding modern high-resolution ARPES experiments, Fig. 7(a) reveals that linear electron densities of up to about $3000e^-$/mm will be tolerable if the space-charge-induced energy broadening and shift are to be kept below ~5 meV. This estimate is in fair agreement with Ref. 9 in which a Fermi-level broadening of ~5 meV was measured for roughly $600e^-$ per pulse and an average spot diameter of 0.37 mm.

In ARPES, however, not only the energy of the emitted electrons is measured, but also their wave vector parallel to the surface $k_\parallel$, which is directly related to the measured kinetic energy E_{kin} and the measured emission angle ϑ by

$$k_\parallel = \sqrt{\frac{2m_e}{\hbar^2}E_{\mathrm{kin}}}\sin\vartheta. \tag{3}$$

Since vacuum space-charge effects will not only distort the energy distribution of the photoelectrons but also their angular distribution, it is clear that, in addition to energy resolution, also momentum resolution $\Delta k_\parallel$ can be lost. It follows from Eq. (3) that, near normal electron emission ($\vartheta \approx 0°$), the momentum resolution is proportional to the angular resolution $\Delta\vartheta$,

$$\Delta k_\parallel \approx \sqrt{\frac{2m_e}{\hbar^2}E_{\mathrm{kin}}}\Delta\vartheta, \tag{4}$$

where $\Delta\vartheta$ now covers the effects of both the finite angular resolution of the spectrometer and the angle blurring due to space charge.

To estimate the loss of momentum resolution in ARPES caused by space charge, we have performed analogous simulations as above, but this time with mean energies $E_i \in \{1, 25, 100\ \mathrm{eV}\}$. As a measure of $\Delta\vartheta$ we have taken the space-charge-induced lateral extension of the electron cloud, as illustrated in the inset of Fig. 7(b).

The computed momentum broadening shows a linear dependence on $N_c/(d_0\sqrt{E_i})$, the number of cloud electrons per pulse divided by the spot diameter and the square root of the initial test electron energy [see Fig. 7(b)]. This functional dependence can be understood as follows. The increase in angular spread is approximately given by $\Delta\vartheta \approx \Delta v_\parallel / v_0$, where $\Delta v_\parallel$ is the surface-parallel velocity spread and v_0 is the group velocity of the test electrons. With the reasonable assumptions that $v_0 \Delta v_\parallel \propto \Delta E_{\mathrm{broad}} \propto N_c$, the space-charge-induced $\Delta\vartheta$ becomes proportional to N_c/E_i and thus, via relation (4), $\Delta k_\parallel \propto N_c/\sqrt{E_i}$.

In modern ARPES, momentum resolutions well below 0.01 $\mathrm{Å}^{-1}$ can be achieved.[10,45,46] As Fig. 7(b) shows, keeping space-charge-induced momentum broadening below this value implies a limit on the electron density of roughly $10\,000e^-/(\mathrm{mm\ eV}^{1/2})$. For photoelectrons emitted from a 0.4 mm spot with a kinetic energy of 30 eV, this means a rather high tolerable number of electrons per pulse of ~22 000. Thus, as regards to space-charge effects in ARPES, one should be much more concerned about loss of energy resolution than loss of momentum resolution. In other words, in typical pulsed ARPES experiments the lateral expansion of the photoelectron cloud is much more critical than its transverse expansion.

In closing this section, we have demonstrated that the mutual Coulomb interaction between the emitted electrons in pulsed photoemission experiments poses an inevitable limit to the achievable energy resolution. But the more important point here is that space-charge-induced energy shifts and broadenings reach values of ~5 meV, a number comparable to the combined energy resolution of modern light sources and electron spectrometers, already at rather low electron densities of $\sim 3000e^-/(\mathrm{pulse\ mm})$ diameter of the light spot.

VI. SUMMARY AND CONCLUSIONS

When more than one electron is ejected from a solid sample in a pulsed photoemission experiment, the emitted electrons will interact via Coulomb repulsion while traveling to the detector. For highly conductive samples, the photoelectrons will also feel the attractive Coulomb forces of their mirror charges inside the sample. Since these space-charge effects directly pertain to the two most important quantities to be measured in photoemission spectroscopy, the kinetic energy and the emission angle of the photoelectron, they need to be considered when ultimate energy and angular resolutions are to be achieved. Moreover, vacuum space-charge effects will be a crucial factor in achieving even moderate resolution when other pulsed photon sources with extreme peak brilliance, for example, free-electron lasers, are used.

Since the magnitude of space-charge effects depends on many source and sample-specific parameters, in particular the number of electrons per pulse, the spot size on the sample, the pulse duration, the initial energy, and angular distribution of the photoelectrons, and since the electron densities at which the effects become significant are expected to be rather low,[9] a molecular-dynamics simulation seems to be the natural approach to a detailed understanding. As we are also interested in the case of rather high electron densities, for which interaction-induced changes in the phase-space distribution of the propagating electron cloud become relevant, we have chosen to perform full N-electron simulations using a modified tree-code algorithm.[41]

We have tested the numerical approach on three recent experimental cases[9,21,40] covering picosecond and femtosecond ultraviolet and extreme ultraviolet photoemission spectroscopies. The experimental results could be reproduced fairly well; larger discrepancies could be ascribed to uncertainties in the experimental parameters. The numerical simulations thus contribute to a better understanding of specific experimental situations. Moreover, they allow us to abstract from these specific experiments and discuss space-charge effects from a more general perspective.

To this end, we have simulated typical experimental situations, representative of core-level as well as valence-band

photoemission spectroscopies, over wide parameter ranges. Not unexpectedly, the number of electrons per pulse and the diameter of the light spot on the sample have turned out as the most crucial factors determining the space-charge-induced energy broadening and shift. The pulse duration (<100 ps in all simulations) and the kinetic energy of the photoelectrons are of much lesser importance. In the numerical simulations, isotropic electron emission and normal-emission detection have been assumed. For a more forwardly directed electron emission, the broadenings and shifts will of course be larger. For example, a cosine angular distribution typically increases energy broadenings and shifts by about 20%–30%. Mirror-charge effects have been included in all simulations of the present work. If they are neglected, the calculated energy broadenings and shifts are about 50%–100% larger for a given parameter set.

The results of the numerical simulations have been compared to simple analytical models. Within the range of parameters typically used in solid-state photoemission, the model introduced by Long *et al.*[37] turns out to be remarkably accurate in predicting the onset of space-charge-induced energy broadening. The mean-field model developed by Siwick *et al.*[25] to describe pulse propagation in ultrafast electron diffraction, on the other hand, is only valid for very low kinetic energies (≤ 1 eV) and femtosecond pulses. The predictions of this latter model may not be extrapolated to higher kinetic energies.[40]

Our comprehensive simulations have finally yielded a few rules of thumb for the onset of space-charge broadening in solid-state photoemission. In core-level spectroscopy (XPS), for the energy broadening to be kept below ~ 50 meV, the pulses must be limited to fewer than $\sim 10\,000 e^-/\mathrm{mm}$ spot diameter. In valence-band spectroscopy (ARPES), the 5 meV resolution limit corresponds to $\sim 3000 e^-/\mathrm{mm}$. A somewhat surprising result is that momentum broadening in ARPES is much less critical. The space-charge-induced momentum broadening is inversely proportional to the square root of the kinetic energy. For the broadening to be smaller than 0.01 Å^{-1} for a 1 mm diameter spot, the pulses must stay below $\sim 10\,000 e^-/\mathrm{eV}^{1/2}$.

In conclusion, our results have clearly confirmed that the mutual Coulomb interaction between emitted electrons poses an elementary limit on energy resolution and, to a much lesser degree, on angular resolution in solid-state photoemission spectroscopy. This limit strongly depends on the brilliance of the photon source. The high-intensity pulses and sharp foci of present and future sources are particularly problematic. Also, time-dependent flux variation is an issue, as it, for example, occurs at third-generation synchrotron-radiation sources without top-off mode on the time scale of hours and at free-electron lasers employing self-amplified spontaneous emission (SASE) on a shot-to-shot basis. Other strategies to avoid space-charge effects in solid-state photoemission are clearly desirable. A rather obvious approach is to combine a high-repetition low-pulse-intensity photon source with a high-resolution electron spectrometer capable of detecting a wide energy range and, at best, the full emission hemisphere in parallel.

ACKNOWLEDGMENTS

This work was motivated by the capabilities of the Free-Electron Laser in Hamburg (FLASH) and supported in part by the Deutsche Forschungsgemeinschaft and the Bundesministerium für Bildung und Forschung. We acknowledge useful discussions with M. Bauer and S. Mathias and we thank M. Kalläne for critical reading of the paper.

[1] *Angle-Resolved Photoemission: Theory and Current Applications*, edited by S. D. Kevan (Elsevier, Amsterdam, 1992).
[2] S. Hüfner, *Photoelectron Spectroscopy: Principles and Applications*, 3rd ed. (Springer, Berlin, 2003).
[3] A. Damascelli, Z. Hussain, and Z.-X. Shen, Rev. Mod. Phys. **75**, 473 (2003).
[4] H. Petek and S. Ogawa, Prog. Surf. Sci. **56**, 239 (1997).
[5] M. Bauer, J. Phys. D **38**, R253 (2005).
[6] G. Margaritondo and F. Cerrina, Nucl. Instrum. Methods Phys. Res. A **291**, 26 (1990).
[7] M. Marsi, L. Casalis, L. Gregoratti, S. Günther, A. Kolmakov, J. Kovac, D. Lonza, and M. Kiskinova, J. Electron Spectrosc. Relat. Phenom. **84**, 73 (1997).
[8] N. Martensson, P. Baltzer, P. A. Brühwiler, J.-O. Forsell, A. Nilsson, A. Stenborg, and B. Wannberg, J. Electron Spectrosc. Relat. Phenom. **70**, 117 (1994).
[9] X. J. Zhou, B. Wannberg, W. L. Yang, V. Brouet, Z. Sun, J. F. Douglas, D. Dessau, Z. Hussain, and Z.-X. Shen, J. Electron Spectrosc. Relat. Phenom. **142**, 27 (2005).
[10] T. Kiss, T. Shimojima, K. Ishizaka, A. Chainani, T. Togashi, T. Kanai, X.-Y. Wang, C.-T. Chen, S. Watanabe, and S. Shin, Rev. Sci. Instrum. **79**, 023106 (2008).
[11] A. L'Huillier and P. Balcou, Phys. Rev. Lett. **70**, 774 (1993).
[12] J. J. Macklin, J. D. Kmetec, and C. L. Gordon, Phys. Rev. Lett. **70**, 766 (1993).
[13] W. Ackermann, G. Asova, V. Ayvazyan, A. Azima, N. Baboi, J. Bähr, V. Balandin, B. Beutner, A. Brandt, A. Bolzmann, R. Brinkmann, O. I. Brovko, M. Castellano, P. Castro, L. Catani, E. Chiadroni, S. Choroba, A. Cianchi, J. T. Costello, D. Cubaynes, J. Dardis, W. Decking, H. Delsim-Hashemi, A. Delserieys, G. Di Pirro, M. Dohlus, S. Düsterer, A. Eckhardt, H. T. Edwards, B. Faatz, J. Feldhaus, K. Flöttmann, J. Frisch, L. Fröhlich, T. Garvey, U. Gensch, Ch. Gerth, M. Görler, N. Golubeva, H.-J. Grabosch, M. Grecki, O. Grimm, K. Hacker, U. Hahn, J. H. Han, K. Honkavaara, T. Hott, M. Hüning, Y. Ivanisenko, E. Jaeschke, W. Jalmuzna, T. Jezynski, R. Kammering, V. Katalev, K. Kavanagh, E. T. Kennedy, S. Khodyachykh, K. Klose, V. Kocharyan, M. Körfer, M. Kollewe, W. Koprek, S. Korepanov, D. Kostin, M. Krassilnikov, G. Kube, M. Kuhlmann, C. L. S. Lewis, L. Lilje, T. Limberg, D. Lipka, F. Löhl, H. Luna, M. Luong, M. Martins, M. Meyer, P. Michelato, V. Miltchev, W. D. Möller, L. Monaco, W. F. O. Müller, O. Napieralski, O. Napoly, P. Nicolosi, D. Nölle, T. Nuñez, A. Oppelt, C. Pagani, R. Paparella, N. Pchalek, J. Pedregosa-Gutierrez, B. Petersen, B. Petrosyan, G. Petrosyan, L. Petrosyan, J. Pflüger, E. Plönjes, L. Poletto, K. Pozniak, E. Prat, D. Proch, P. Pucyk, P. Radcliffe, H.

Redlin, K. Rehlich, M. Richter, M. Roehrs, J. Roensch, R. Romaniuk, M. Ross, J. Rossbach, V. Rybnikov, M. Sachwitz, E. L. Saldin, W. Sandner, H. Schlarb, B. Schmidt, M. Schmitz, P. Schmüser, J. R. Schneider, E. A. Schneidmiller, S. Schnepp, S. Schreiber, M. Seidel, D. Sertore, A. V. Shabunov, C. Simon, S. Simrock, E. Sombrowski, A. A. Sorokin, P. Spanknebel, R. Spesyvtsev, L. Staykov, B. Steffen, F. Stephan, F. Stulle, H. Thom, K. Tiedtke, M. Tischer, S. Toleikis, R. Treusch, D. Trines, I. Tsakov, E. Vogel, T. Weiland, H. Weise, M. Wellhöfer, M. Wendt, I. Will, A. Winter, K. Wittenburg, W. Wurth, P. Yeates, M. V. Yurkov, I. Zagorodnov, and K. Zapfe, Nat. Photonics **1**, 336 (2007).

[14] R. Haight and D. R. Peale, Rev. Sci. Instrum. **65**, 1853 (1994).

[15] P. Siffalovic, M. Drescher, M. Spieweck, T. Wiesenthal, Y. C. Lim, R. Weidner, A. Elizarov, and U. Heinzmann, Rev. Sci. Instrum. **72**, 30 (2001).

[16] M. Bauer, C.-F. Lei, K. Read, R. Tobey, J. Gland, M. M. Murnane, and H. C. Kapteyn, Phys. Rev. Lett. **87**, 025501 (2001).

[17] P. Siffalovic, M. Drescher, and U. Heinzmann, Europhys. Lett. **60**, 924 (2002).

[18] A. L. Cavalieri, N. Müller, Th. Uphues, V. S. Yakovlev, A. Baltuska, B. Horvath, B. Schmidt, L. Blümel, R. Holzwarth, S. Hendel, M. Drescher, U. Kleineberg, P. M. Echenique, R. Kienberger, F. Krausz, and U. Heinzmann, Nature (London) **449**, 1029 (2007).

[19] S. Mathias, L. Miaja-Avila, M. M. Murnane, H. C. Kapteyn, M. Aeschlimann, and M. Bauer, Rev. Sci. Instrum. **78**, 083105 (2007).

[20] L. Miaja-Avila, G. Saathoff, S. Mathias, J. Yin, C. La-o-vorakiat, M. Bauer, M. Aeschlimann, M. M. Murnane, and H. C. Kapteyn, Phys. Rev. Lett. **101**, 046101 (2008).

[21] A. Pietzsch, A. Föhlisch, M. Beye, M. Deppe, F. Hennies, M. Nagasono, E. Suljoti, W. Wurth, C. Gahl, K. Döbrich, and A. Melnikov, New J. Phys. **10**, 033004 (2008).

[22] H. Boersch, Z. Phys. **139**, 115 (1954).

[23] T. Srinivasan-Rao, J. Fischer, and T. Tsang, J. Appl. Phys. **69**, 3291 (1991).

[24] M. Woods, J. Clendenin, J. Frisch, A. Kulikov, P. Saez, D. Schultz, J. Turner, K. Witte, and M. Zolotorev, J. Appl. Phys. **73**, 8531 (1993).

[25] B. J. Siwick, J. R. Dwyer, R. E. Jordan, and R. J. D. Miller, J. Appl. Phys. **92**, 1643 (2002).

[26] B. W. Reed, J. Appl. Phys. **100**, 034916 (2006).

[27] G. A. Massey, M. D. Jones, and B. P. Plummer, J. Appl. Phys. **52**, 3780 (1981).

[28] J. Bokor, R. Haight, R. H. Storz, J. Stark, R. R. Freeman, and P. H. Bucksbaum, Phys. Rev. B **32**, 3669 (1985).

[29] R. Clauberg and A. Blacha, J. Appl. Phys. **65**, 4095 (1989).

[30] C. Girardeau-Montaut, J. P. Girardeau-Montaut, and H. Leboutet, Appl. Phys. Lett. **55**, 2556 (1989).

[31] T. L. Gilton, J. P. Cowin, G. D. Kubiak, and A. V. Hamza, J. Appl. Phys. **68**, 4802 (1990).

[32] Gy. Farkas and C. Toth, Phys. Rev. A **41**, 4123 (1990).

[33] C. Girardeau-Montaut and J. P. Girardeau-Montaut, Phys. Rev. A **44**, 1409 (1991).

[34] M. V. Ammosov, J. Opt. Soc. Am. B **8**, 2260 (1991).

[35] P. Martin, R. Trainham, P. Agostini, and G. Petite, Phys. Rev. B **45**, 69 (1992).

[36] G. Petite, P. Agostini, R. Trainham, E. Mevel, and P. Martin, Phys. Rev. B **45**, 12210 (1992).

[37] J. P. Long, B. S. Itchkawitz, and M. N. Kabler, J. Opt. Soc. Am. B **13**, 201 (1996).

[38] B. Wannberg, P. Baltzer, and S. Shin (unpublished).

[39] D. M. Riffe, X. Y. Wang, M. C. Downer, D. L. Fisher, T. Tajima, J. L. Erskine, and R. M. More, J. Opt. Soc. Am. B **10**, 1424 (1993).

[40] S. Passlack, S. Mathias, O. Andreyev, D. Mittnacht, M. Aeschlimann, and M. Bauer, J. Appl. Phys. **100**, 024912 (2006).

[41] J. Barnes and P. Hut, Nature (London) **324**, 446 (1986).

[42] http://ifa.hawaii.edu/~barnes/treecode/treeguide.html

[43] F. Reinert, G. Nicolay, S. Schmidt, D. Ehm, and S. Hüfner, Phys. Rev. B **63**, 115415 (2001).

[44] A. Bytchkov, A. A. Fateev, J. Feldhaus, U. Hahn, M. Hesse, U. Jastrow, V. Kocharyan, N. I. Lebedev, E. A. Matyushevskiy, E. L. Saldin, E. A. Schneidmiller, A. V. Shabunov, K. P. Sytchev, K. Tiedtke, R. Treusch, and M. V. Yurkov, Nucl. Instrum. Methods Phys. Res. A **528**, 254 (2004).

[45] E. Rotenberg, H. Koh, K. Rossnagel, H. W. Yeom, J. Schäfer, B. Krenzer, M. P. Rocha, and S. D. Kevan, Phys. Rev. Lett. **91**, 246404 (2003).

[46] J. D. Koralek, J. F. Douglas, N. C. Plumb, Z. Sun, A. V. Federov, M. M. Murnane, H. C. Kapteyn, S. T. Cundiff, Y. Aiura, K. Oka, H. Eisaki, and D. S. Dessau, Phys. Rev. Lett. **96**, 017005 (2006).